Local Energetics Analysis of Blocking Formation in the North Pacific Decomposed in Vertical Mean and Sheared Flows

Yasushi WATARAI

Terrestrial Environment Research Center, University of Tsukuba, Tsukuba, Japan

and

H.L. TANAKA

Life and Environmental Sciences, University of Tsukuba, Tsukuba, Japan
Frontier Research Center for Global Change, Japan Agency for Marine-Earth Science and Technology, Yokohama, Japan

(Manuscript received 12 January 2004, in final form 28 May 2004)

Journal of the Meteorological Society of Japan
Vol. 82, No. 5
Meteorological Society of Japan

NOTES AND CORRESPONDENCE

Local Energetics Analysis of Blocking Formation in the North Pacific Decomposed in Vertical Mean and Sheared Flows

Yasushi WATARAI

Terrestrial Environment Research Center, University of Tsukuba, Tsukuba, Japan

and

H.L. TANAKA

Life and Environmental Sciences, University of Tsukuba, Tsukuba, Japan
Frontier Research Center for Global Change, Japan Agency for Marine-Earth Science and Technology, Yokohama, Japan

(Manuscript received 12 January 2004, in final form 28 May 2004)

Abstract

In this study, local energetics analysis is conducted for the blocking formation in the North Pacific, in order to investigate the condition of a transient ridge to become a blocking. Among the total number of 452 ridges, 88 are identified as blocking during 51 winters from 1950 to 2001. Kinetic energy budget is then performed in the framework of the vertical mean and sheared flows, and the energetics terms, including the barotropic-baroclinic interactions, $C(K_s, K_m)$, are analyzed.

As a result, we find that a blocking becomes Ω type for large $C(K_s, K_m)$, and it becomes dipole type for small $C(K_s, K_m)$. It is also shown for the large $C(K_s, K_m)$, that a ridge develops to a blocking when the flux convergence of mechanical energy of the mean flow, $B(K_m + \phi_m)$, is positive around the ridge. On the contrary, a ridge flows away downstream when $B(K_m + \phi_m)$ is negative there. The positive $B(K_m + \phi_m)$ around the blocking is associated with the enhanced negative $B(K_m + \phi_m)$ at the upstream jet, due to the intensified mechanical energy flux from the upstream jet. Therefore, it is found that the sign of the flux convergence of mechanical energy around the transient ridge is the condition for the ridge to become a blocking.

1. Introduction

Atmospheric blocking is a long-lived, quasi-stationary, and equivalent-barotropic anticyclone, which has a larger spatial scale than synoptic eddies. For its peculiar configuration, stagnation, and persistence, the blocking causes an abnormal weather for a week or more. Moreover, blocking phenomenon can be a significant source, which the forecast skill falls off. Especially, it is difficult to predict the blocking state near the onset time (Kimoto et al. 1992).

For the blocking formation and the maintenance, a large number of papers were published for the last 50 years. Shutts (1983) clearly demonstrated, using a barotropic model, that barotropic eddies superimposed on a split-

Corresponding author: Yasushi Watarai, Terrestrial Environment Research Center, University of Tsukuba, Tsukuba 305-8577, Japan.
E-mail: watarai@suiri.tsukuba.ac.jp

jet basic flow, can maintain the blocking pattern. The eddy straining hypothesis advocated by him is supported by many studies. For example, Mullen (1987) examined the composite of 17 blocking events in the North Atlantic using a geopotential tendency equation. He exhibited that synoptic eddies brought the anticyclonic forcing to the one-quarter wavelength upstream of the blocking ridge. Haines and Marshall (1987) demonstrated a 'modon' as a prototype of the blocking using an equivalent barotropic model, and Tanaka (1998) simulated the realistic blockings on a sphere, using a simple barotropic model with parameterized baroclinic instability. Each of them showed that the blocking is maintained by the supply of low (high) potential vorticity at the north (south), due to the transient eddies. From the viewpoint of energetics, the eddy straining process for the blocking formation corresponds to the upscale energy cascade from synoptic waves to planetary waves, which is shown by many studies (e.g., Hansen and Sutera 1984; Kung and Baker 1986; Tanaka and Kung 1988). Tanaka and Kung (1988) performed the global energetics analysis by the three-dimensional normal mode technics. They found the energy transformation from the synoptic-scale baroclinic component, to the planetary-scale barotropic component, prior to the onset of blocking. This result suggests the importance of the contribution from the barotropic-baroclinic interactions during the formation of blocking.

Watarai and Tanaka (2002) (hereafter WT) examined the characteristics of the barotropic-baroclinic interactions in the kinetic energy equations divided in the vertical mean and sheared flows. They showed by case studies and the composite analysis of 10 blockings, that the barotropic-baroclinic interactions are intensified in both the western and eastern flanks of the blocking ridge. The result suggests the importance of the energy flow from baroclinic to barotropic components during the formation of a blocking (Tanaka and Kung 1988). However, there are cases such that a blocking occurred without the barotropic-baroclinic interactions, or a ridge did not develop to a blocking despite the appearance of large barotropic-baroclinic interactions. A further analysis is required to investigate the condition of a transient ridge to become a blocking.

The objective of this study is to investigate the condition of a transient ridge to become a blocking based on a comprehensive energetics analysis using a number of samples. As in WT, kinetic energy budget is performed in the framework of the vertical mean and sheared flows, and all energetics terms, including the barotropic-baroclinic interactions, are analyzed.

Section 2 describes the local kinetic energy equations decomposed in mean and sheared flows. The definition of the blocking event, and the quantification of barotropic-baroclinic interactions are presented in section 3. Section 4 describes the data used in this study. The results of energetics analysis for blocking and non-blocking cases in the North Pacific, are presented in section 5. Finally, discussion and conclusions are given in section 6.

2. Local kinetic energy equations

In this study, we used the local formulation of kinetic energy equations, separated in the vertical mean (barotropic) and sheared (baroclinic) flows. The method was first formulated for global-mean equations by Wiin-Nielsen (1962). He also extended it to the zonal-wavenumber domain. Chen and Yen (1985) extended Wiin-Nielsen's formulation to the local budget of barotropic and baroclinic kinetic energies. In this study, we computed the local kinetic energy budget following Chen and Yens' formulation as in WT.

According to WT, kinetic energy of the vertical mean (K_m), and sheared (K_s) flows, integrated with respect to the vertical are governed by the following equations:

$$\frac{\partial K_m}{\partial t} = B(K_m) + G(K_m) + C(K_s, K_m) - D(K_m), \tag{1}$$

$$\frac{\partial K_s}{\partial t} = B(K_s) + G(K_s) - C(K_s, K_m) - D(K_s), \tag{2}$$

where the subscripts m and s designate the vertical mean and sheared components, respectively. These are defined by the following operation for a field variable ξ:

$$\xi_m = \frac{1}{p_s}\int_0^{p_s} \xi\, dp, \quad \xi_s = \xi - \xi_m, \tag{3}$$

where p_s is the surface pressure. Hereafter, the vertical mean and sheared components are referred to as barotropic and baroclinic components, respectively. Terms B, G, C and D are the horizontal flux convergence of kinetic energy, the kinetic energy generation by the cross-isobaric flow, the conversion from the baroclinic component to the barotropic component, and the dissipation of kinetic energy, respectively.

The barotropic-baroclinic interactions, $C(K_s, K_m)$, is the only connection between the barotropic and baroclinic kinetic energies. This term can be decomposed in the divergent and nondivergent parts:

$$C(K_s, K_m) = C_D(K_s, K_m) + C_{ND}(K_s, K_m), \quad (4)$$

where

$$C_D(K_s, K_m) = -\frac{p_s}{g}\{(\mathbf{V}_m \cdot \mathbf{V}_s)\nabla \cdot \mathbf{V}_s\}_m, \quad (5)$$

$$C_{ND}(K_s, K_m) = -\frac{p_s}{g}\{\mathbf{V}_m \cdot (\mathbf{k} \times \mathbf{V}_s)\zeta_s\}_m. \quad (6)$$

The term $\mathbf{V}$ is the horizontal wind vector, g the acceleration of gravity, ζ the relative vorticity, and $\mathbf{k}$ the vertical unit vector.

The sum of the flux convergence of kinetic energy, $B(K_m)$, and the generation of kinetic energy, $G(K_m)$, in the barotropic flow can be written as

$$\begin{aligned} &B(K_m) + G(K_m) \\ &= -\frac{p_s}{g}(\nabla \cdot k\mathbf{V}_m)_m - \frac{p_s}{g}\mathbf{V}_m \cdot \nabla\phi_m \\ &= -\frac{p_s}{g}\{\nabla \cdot (k + \phi_m)\mathbf{V}_m\}_m \\ &= B(K_m + \phi_m), \end{aligned} \quad (7)$$

where k and ϕ are kinetic energy and geopotential, respectively. Here the divergence vanishes for the barotropic flow, since it is assumed that the vertical p-velocity, ω, is zero at the top and bottom boundaries. The term $B(K_m + \phi_m)$ represents the flux convergence of mechanical energy (i.e., the sum of kinetic energy and potential energy) in the barotropic flow.

On the other hand, the sum of $B(K_s)$ and $G(K_s)$ included in Eq. (2) can be written as

$$\begin{aligned} &B(K_s) + G(K_s) \\ &= -\frac{p_s}{g}(\nabla \cdot k\mathbf{V}_s)_m - \frac{p_s}{g}(\mathbf{V}_s \cdot \nabla\phi_s)_m \\ &= -\frac{p_s}{g}\{\nabla \cdot (k + \phi_s)\mathbf{V}_s\}_m - \frac{p_s}{g}(\omega_s\alpha_s)_m \\ &= B(K_s + \phi_s) + C(A, K_s), \end{aligned} \quad (8)$$

where α is the specific volume, and A the available potential energy. The term $B(K_s + \phi_s)$ represents the flux convergence of mechanical energy in the baroclinic flow, and $C(A, K_s)$ is the baroclinic conversion from available potential energy to baroclinic kinetic energy.

3. Definition of indices

3.1 The B-index

In order to identify many blocking events objectively, a "B-index" defined by Lejenäs and Økland (1983), is employed in this study. The B-index is defined as the local difference in 500-hPa geopotential height at 40°N, subtracted from that at 60°N. When the B-index is negative, as seen for a high-pressure cell staying around 60°N, the situation is considered as a low-index event. The onset of the low-index event is defined in the Hovmöller diagram (not shown) when the B-index first shows a negative value, and a duration is measured by the period for the negative B-index. Here, the index is averaged from −10° to +10° along the longitude to filter the small scale noise when the onset and the duration are measured.

Each of low-index event has a variety of duration, so a low-index event is not always regarded as a blocking. Therefore, a low-index event lasting at least 7 days, is defined as a blocking event in this study. Conversely, an event lasting less than 3 days is considered as a non-blocking event. Since we are interested in blocking events in the North Pacific sector, only the low-index events occurred between 140°E and 130°W are picked up. The total of 452 low-index events are extracted during the 51 winters from 1950 to 2001. Among those, 88 events are identified as blocking and 253 events as non-blocking events.

3.2 The C-index

The barotropic-baroclinic interactions, $C(K_s, K_m)$, plays an important role when a blocking occurs. By examining 10 typical

blocking events, WT showed two maxima of $C(K_s,K_m)$ appearing along the western and eastern flanks of the blocking anticyclone. In order to represent the intensity of the barotropic-baroclinic interactions around a blocking, a "C-index" is introduced in this study. The value of $C(K_s,K_m)$ is computed by Eq. (4) at each grid. Since stronger wind makes larger kinetic energy, $C(K_s,K_m)$ tends to have a large magnitude around a blocking compared to that in the blocking. For this reason, we calculated the average of $C(K_s,K_m)$ over $-30°$ to $+30°$ in longitude, and 50° to 70°N in latitude, from the center of the B-index minimum. The "C-index" is then defined by the time average of that term for 3 days before and after the onset of the low-index event in order to filter the transient noise.

4. Description of data

The data used in this study are the reanalysis of the National Center for Environmental Prediction (NCEP)/National Center for Atmospheric Research (NCAR) for 51 winter seasons (November to March) from 1950/51 to 2000/01, with the time interval of six hours (Kalnay et al. 1996). The grid resolution of the data is 2.5° by 2.5° of zonal/meridional directions, and 17 pressure levels at 1000, 925, 850, 700, 600, 500, 400, 300, 250, 200, 150, 100, 70, 50, 30, 20 and 10 hPa.

We mainly focus on the fields separated in barotropic and baroclinic components. In this study, the three-dimensional normal mode expansion technique (Kasahara and Puri 1981; Tanaka 1985) is employed to evaluate these components expanded in the vertical normal modes, which manipulates the zonal wind, meridional wind and geopotential height fields. The barotropic component is approximated by the barotropic mode, and the baroclinic component is evaluated by the sum of the baroclinic modes.

We used 500-hPa geopotential height fields of the NCEP/NCAR reanalysis in order to find blocking events as mentioned above. To grasp the spatial patterns of composite fields, geopotential height and potential vorticity (PV) at 250 hPa will be shown. Following the method of Nakamura and Wallace (1993), an approximated form of PV at 250 hPa is calculated by geopotential height field at 250 hPa, and temperature fields at 200 and 300 hPa of the reanalysis data.

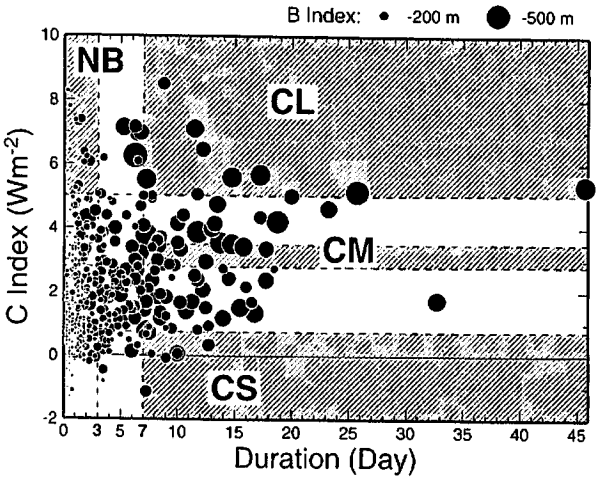

Fig. 1. Relationship between the duration of negative B-index (abscissa) and the magnitude of C-index (ordinate). A radius of closed circle stands for the magnitude of B-index at the mature time, and its legends are the upper right outside the diagram. The shaded areas labeled CL, CM, CS and NB show the zones of four composites defined in the text.

5. Results

Figure 1 illustrates the distribution of the low-index events plotted as functions of the duration of the low-index events, and the value of the C-index. Additionally, the magnitude of the B-index at the mature stage (i.e., the intensity of the event) is represented by the radius of the circle. While almost all the non-blocking events have small circles, the blocking events with the duration longer than 7 days tend to have large circles. The correlation coefficient between the duration and the intensity is 0.74 for all the low-index events. On the other hand, the correlation coefficient between the C-index and the duration (intensity) is 0.20 (0.27) for all the low-index events, which is significant at 99% confidence limit. In general, large blockings are accompanied by the strong value of $C(K_s,K_m)$. To examine the features of the blocking patterns with various values of $C(K_s,K_m)$, the blocking cases having the 10 largest C-index are selected and labeled "CL". The value of the

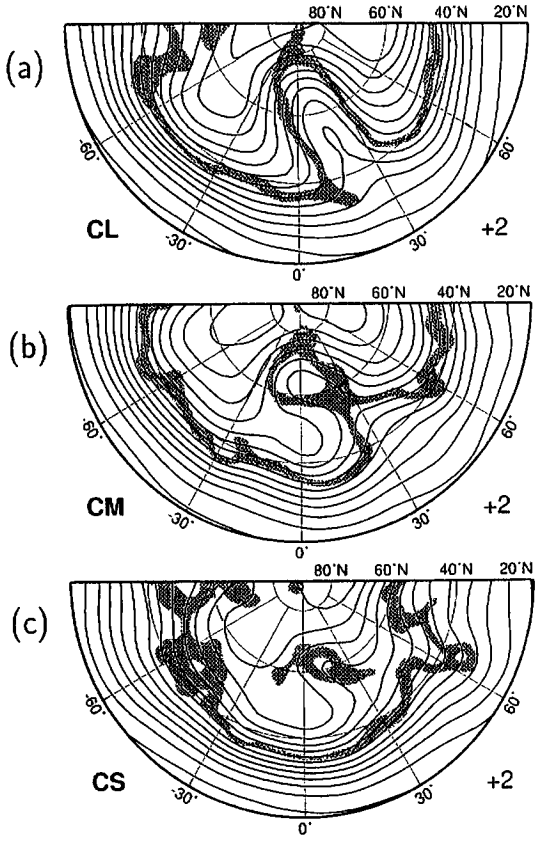

Fig. 2. Composite maps of geopotential height (solid lines) and the approximated isobaric PV ranged from 3 to 4 PVU (shading) at 250-hPa level at +2 days relative to the onset time for (a) CL, (b) CM and (c) CS. The longitude is represented by the relative one from the center of the B-index minimum. Contour interval is 100 m.

C-index is more than 5.02 Wm^{-2} for the CL cases. For comparison, 10 blockings with the smallest C-index are chosen and named "CS", and 10 blockings with the medium C-index as "CM". The mean values of C-index for CM and CS are 3.16 Wm^{-2} and 0.21 Wm^{-2}, respectively. The areas contained in the CL, CM and CS events are shown by shading in Fig. 1.

Figure 2 illustrates a comparison of the composite maps of geopotential height and PV for CL, CM and CS, respectively, at +2 days from the onset time. The composites are based on the longitude of the B-index minimum. In CL, the spatial pattern shows a pronounced blocking of the Ω type with strong poleward jet. On the other hand, the composite of CM shows a typical dipole-type blocking. The poleward jet in CM is weaker than that in CL. The ridge in CS is even weaker, and the spatial pattern is hardly recognized as a blocking. It therefore indicates that the larger the C-index is, the stronger the blocking ridge grows.

As shown in Fig. 1, however, there are cases of non-blocking events in spite of the large values of the C-index. Therefore, the comparison between the blocking and non-blocking cases may bring useful information concerning the blocking formation for the large value of the C-index. Figure 3 shows the composite maps of all the CL cases. Left maps show the geopotential height (contour) and the approximated isobaric PV (shade) at 250-hPa level, and right maps show the corresponding barotropic kinetic energy, K_m. All composite maps are based on the longitude of the B-index minimum. There is a small low-PV disturbance about −10° from the central longitude at day −2. The disturbance amplifies rapidly and moves eastward slowly. At day 0 (the onset time), low-PV air thrusts northwestward and the upstream high-PV air southeastward. The inversion of the north-south PV gradient is formed about 0° longitude. Afterwards, the ridge amplifies more largely, the jet stream splits in north and south, and the Ω-type blocking is formed. The low-PV air corresponding to the blocking is deeply plunged into the poleward air. The blocking formed at about 15° longitude is almost stationary. The diffluence of the jet is evident after day 0. In the poleward jet, the maximum value of K_m is about 3.5×10^6 Jm^{-2}, which is comparable with the equatorward jet. K_m around the upstream jet, which is located at −45° longitude, is the most intense at day −2, exceeding 6×10^6 Jm^{-2}, but it reduces to 5×10^6 Jm^{-2} after the onset time.

Figure 4 shows the composite maps of 250-hPa geopotential height, 250-hPa PV, and K_m associated with "NB" cases. The NB contains the non-blocking cases having the 21 largest C-index. At the onset time (day 0), 250-hPa geopotential height and PV fields are similar to the CL composite, and the inversion of meridional PV gradient occurs at 0° longitude. Although the low-PV air intrudes deeply into high latitudes, the ridge moves eastward and becomes narrower. Finally, the low-PV air squashes, the ridge is attenuated, and the flow about 30° lon-

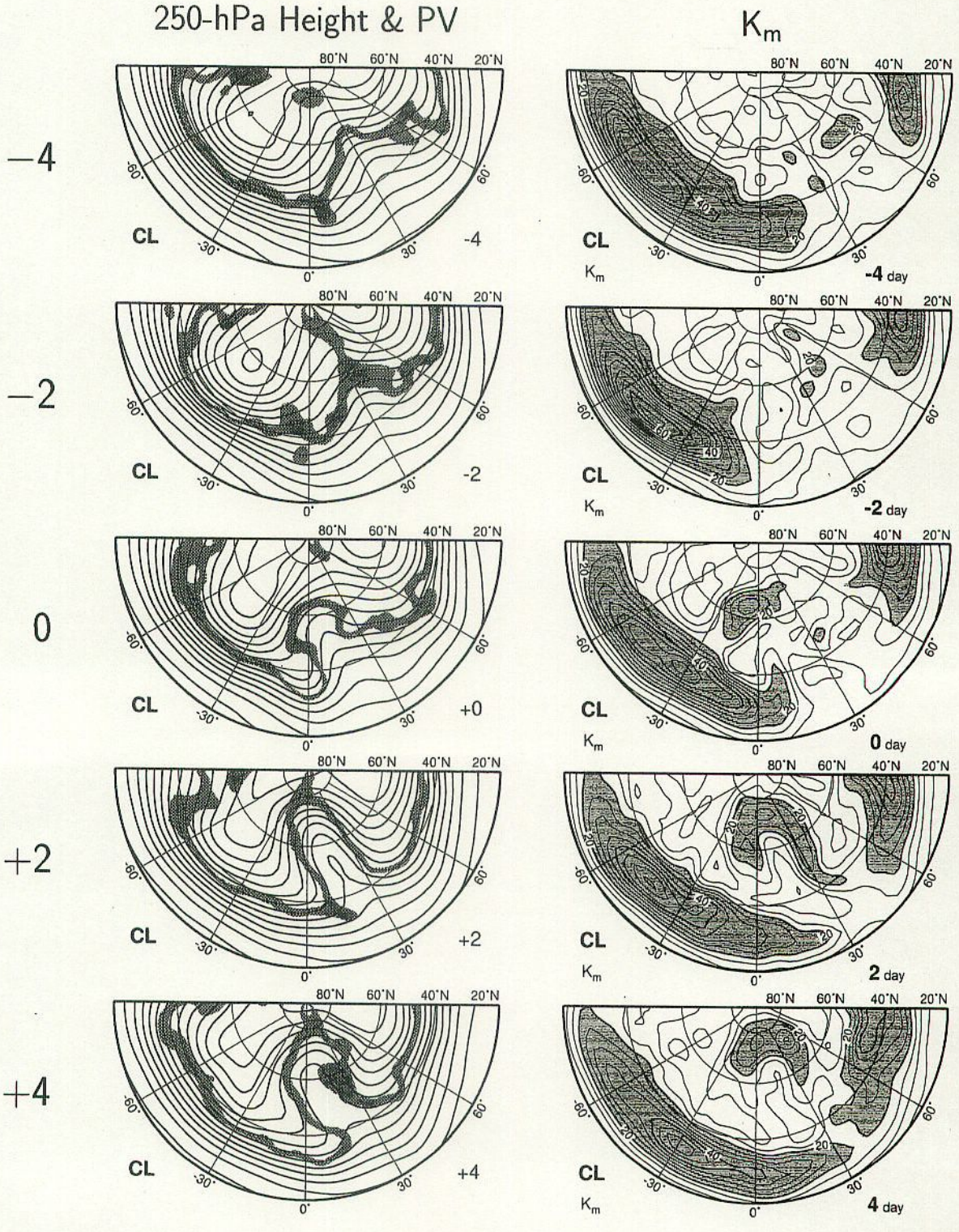

Fig. 3. CL composite maps of geopotential height at 250-hPa level (left; solid lines) and barotropic kinetic energy, K_m (right; solid lines), with a range from −90° to 90° in longitude and 20°N to 90°N in latitude. The longitude is represented by the relative one from the center of the B-index minimum. Shaded areas of left panels show the approximated isobaric PV at 250-hPa level (Nakamura and Wallace 1993), ranged from 3 to 4 PVU (= 10^{-6} $m^2s^{-1}K$ kg^{-1}). Shaded areas of right panels denote the values of K_m exceeding 2×10^6 Jm^{-2}. Contour intervals are 100 m in 250-hPa geopotential height and 5×10^5 Jm^{-2} in K_m. Maps at −4 (top), −2, 0, +2 and +4 (bottom) day(s) from the onset time are displayed.

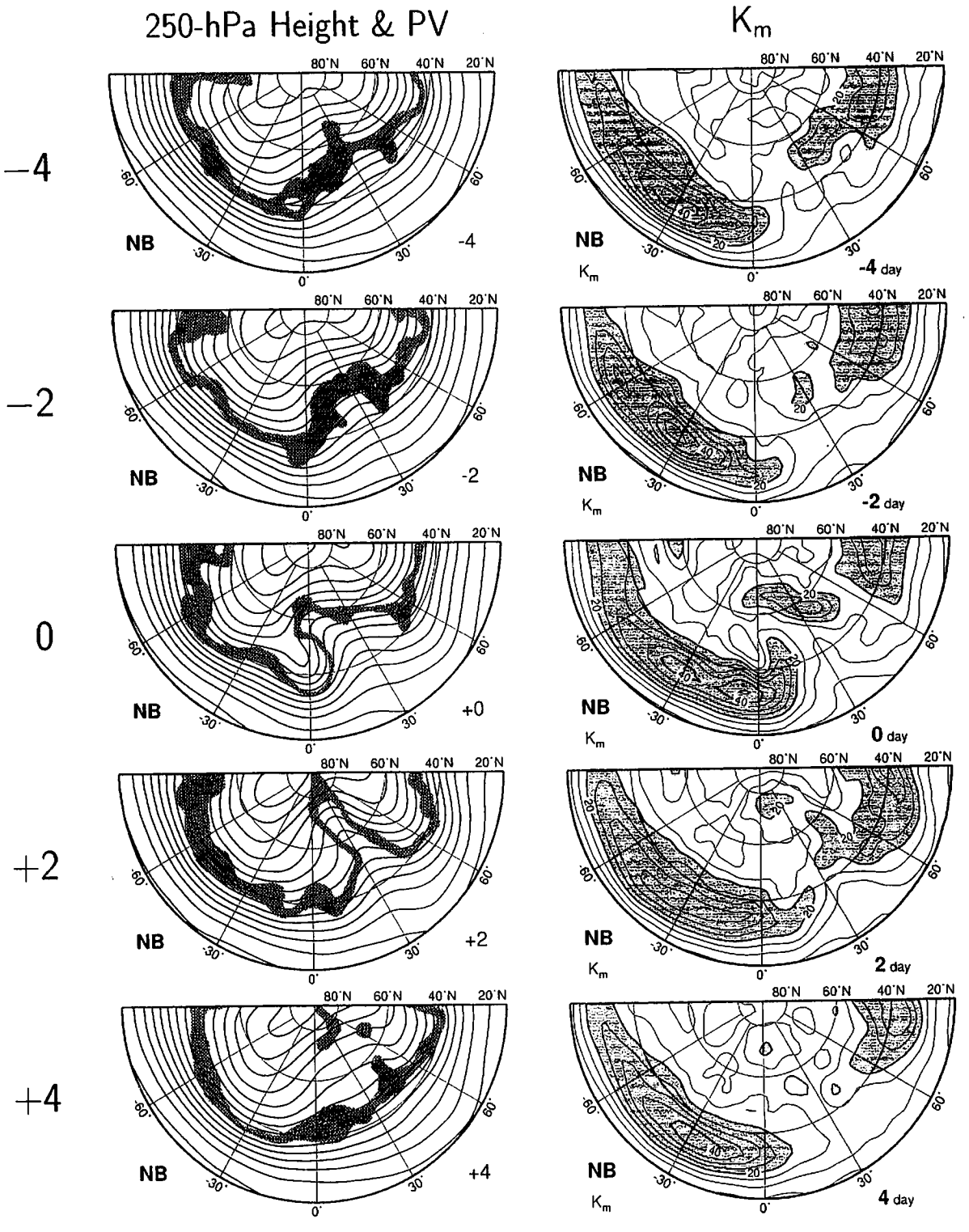

Fig. 4. As in Fig. 3 except for NB composite.

gitude becomes more zonally. The maps of K_m show the meandering of the jet around 30° longitude at day 0, but the double-jet pattern is not formed, and the flow about 30° longitude weakens afterwards. Unlike CL, K_m around the upstream jet doesn't have the marked enhancement prior to the onset time, and keeps about 4×10^6 Jm^{-2} from day −4 to +4.

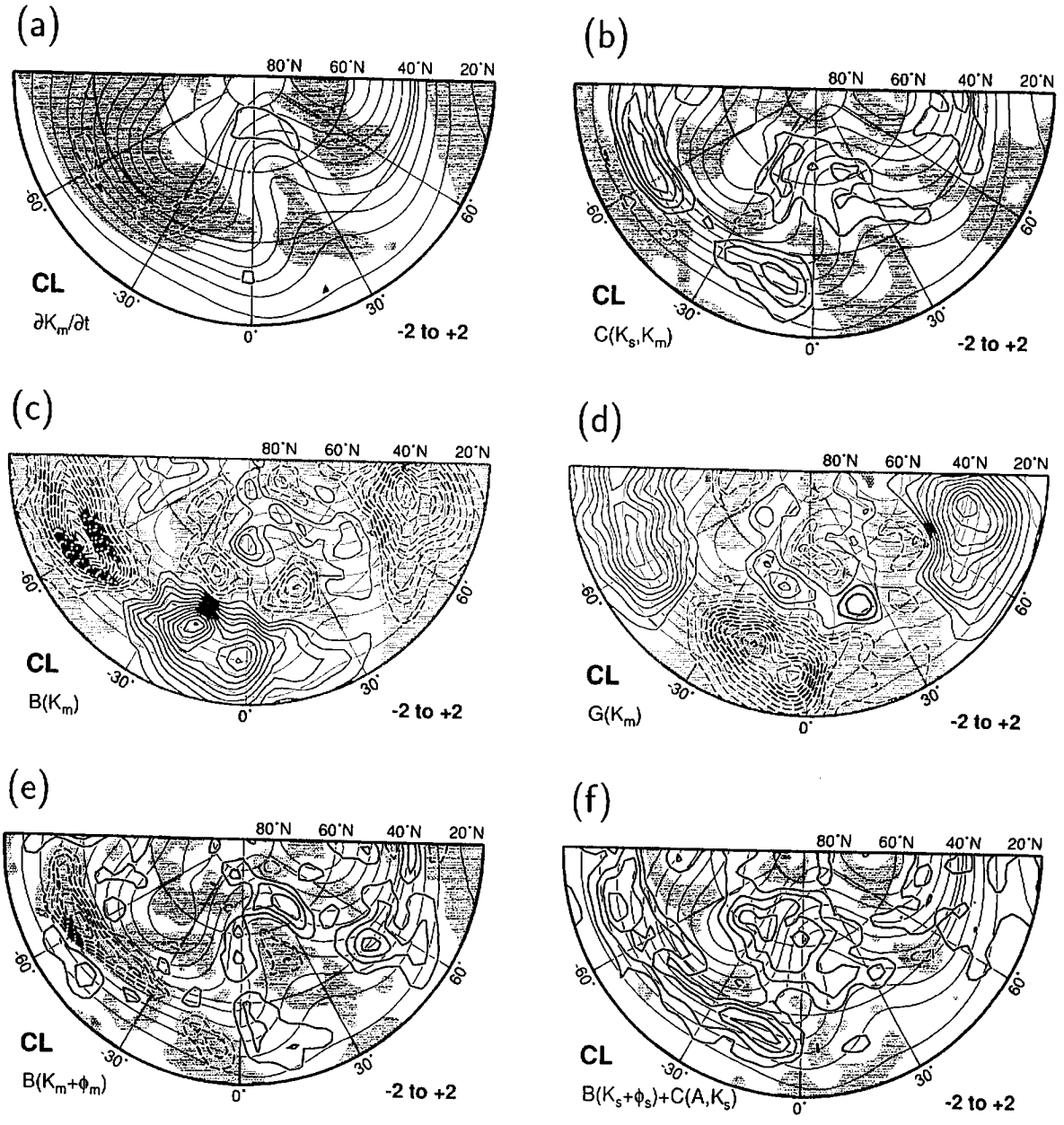

Fig. 5. CL composite of (a) the tendency of barotropic kinetic energy, $\partial K_m/\partial t$; (b) the barotropic-baroclinic interactions, $C(K_s, K_m)$; (c) the convergence term of kinetic energy flux in the barotropic flow, $B(K_m)$; (d) the generation term of barotropic kinetic energy, $G(K_m)$; (e) the flux convergence of mechanical energy in the barotropic flow, $B(K_m + \phi_m)$; and (f) the sum of the flux convergence of mechanical energy in the baroclinic flow, $B(K_s + \phi_s)$, and the conversion from available potential energy to baroclinic kinetic energy, $C(A, K_s)$, averaged from -2 to $+2$ days relative to the onset time. The longitude is represented by the relative one from the center of the B-index minimum. Thick solid contours are positive, thick dashed contours are negative, zero contour is omitted, and shaded areas indicate negative values. Contour interval is 4 Wm^{-2}. Each panel superposes CL composite of 500-hPa geopotential height averaged at the same period (thin solid lines; 75 m interval).

Figure 5 shows the CL composite maps for the terms in Eqs. (1) and (2), averaged from day -2 to $+2$. The tendency of K_m (Fig. 5a) is positive around the ridge and negative around the upstream jet. $C(K_s, K_m)$ (Fig. 5b) is the largest in the entrance of the upstream jet about $-60°$

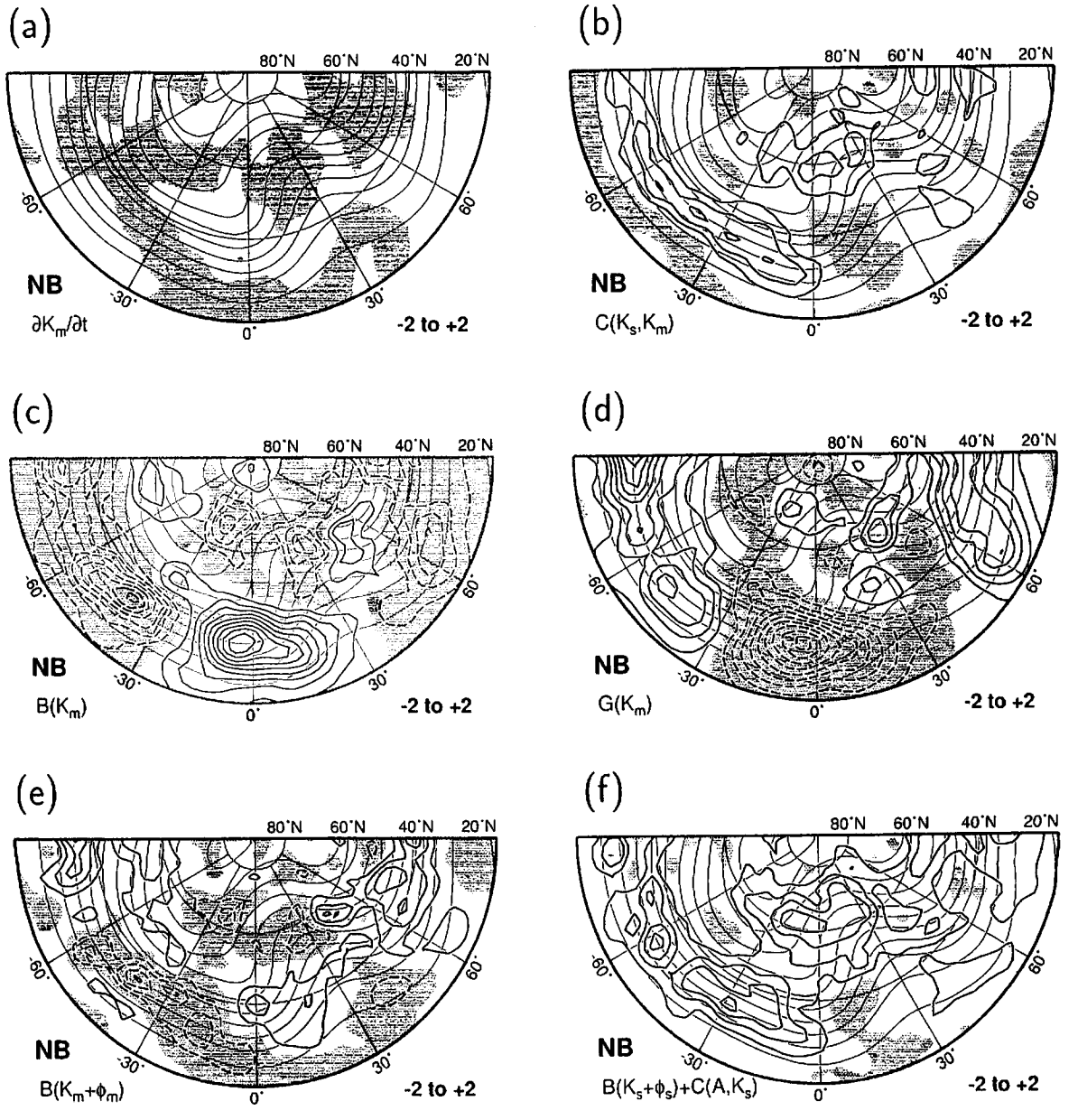

Fig. 6. As in Fig. 5 except for NB composite.

longitude. The second maximum of $C(K_s, K_m)$ is seen around the ridge, which is about a half of the upstream jet. Figure 5(c) and 5(d) show $B(K_m)$ and $G(K_m)$, respectively. The magnitudes of $B(K_m)$ and $G(K_m)$ are about 2 to 3 times larger than $C(K_s, K_m)$. There is, however, a strong cancellation between $B(K_m)$ and $G(K_m)$, as indicated by Chen and Lee (1983) and Chen and Yen (1985). As a result, the magnitude of $B(K_m + \phi_m)$ (Fig. 5e) is comparable to that of $C(K_s, K_m)$. $B(K_m + \phi_m)$ has a positive contribution along the strong-wind region around the ridge, while it is negative on the calm center of the ridge. The upstream jet region corresponds to the strong negative $B(K_m + \phi_m)$. $B(K_s + \phi_s) + C(A, K_s)$ is almost as large as $C(K_s, K_m)$ around the upstream jet, but about twice as large as $C(K_s, K_m)$ around the ridge.

Figure 6 shows the composite maps of the terms in Eqs. (1) and (2) for the NB cases averaged from day -2 to $+2$. Unlike CL, K_m

tends to decrease around the ridge (Fig. 6a). $C(K_s,K_m)$ has maxima around the upstream jet and around the ridge, which is similar to CL (Fig. 6b). The maximum of $C(K_s,K_m)$ is comparable with CL around the ridge. It is about a half of CL at the entrance of the upstream jet (about −60° longitude). It is noteworthy that $B(K_m)$ is negative around the ridge (Fig. 6c) in the opposite sense of CL. As a result, $B(K_m+\phi_m)$ is also negative at this area (Fig. 6e). Around the upstream jet, a negative $B(K_m+\phi_m)$ area is weaker, and more eastward than that in CL. The pattern of $B(K_s+\phi_s)+C(A,K_s)$ is similar to $C(K_s,K_m)$, and $B(K_s+\phi_s)+C(A,K_s)$ is about twice as large as $C(K_s,K_m)$ (Fig. 6f).

Both in CL and in NB, the maximum value of $C(K_s,K_m)$ is located in the upstream jet, and in phase with the maximum of $B(K_s+\phi_s)+C(A,K_s)$. Although they are similar between the pattern of $B(K_m)$ and $B(K_s)$, and between $G(K_m)$ and $G(K_s)$ (not shown), $B(K_s+\phi_s)+C(A,K_s)$ is positive, while $B(K_m+\phi_m)$ is negative around the upstream jet. A positive $B(K_s+\phi_s)+C(A,K_s)$ in this area is due to a positive $G(K_s)$ exceeding a negative $B(K_s)$. Hence, the upstream jet may have strong $C(A,K_s)$, which is included in $G(K_s)$. Therefore, it is indicated that the K_s, converted from A, is in situ transformed into K_m via $C(K_s,K_m)$, around the upstream jet. This process is just a baroclinic conversion. The same feature appears around the ridge.

Figure 7 shows the time series of the terms in Eq. (1) averaged in the ridge area (−30° to 45° in longitude, and 50°N to 80°N in latitude) for (a) CL and (b) NB composites. In both composites, positive K_m tendency (dashed line) gradually increases toward the onset and reaches about 3 Wm^{-2} at the onset time. After the onset, K_m tendency decreases in both composites, but NB decreases more rapidly than CL. Since the selected cases have large values of C-index in both cases, these two composites are similar in the time series of $C(K_s,K_m)$. However, the time series of $B(K_m+\phi_m)$ (thick solid line) is different between CL and NB. In CL, $B(K_m+\phi_m)$ is roughly zero or positive during the period shown in Fig. 7. It is comparable to $C(K_s,K_m)$ at the onset, and is about zero after day +2. In NB, on the other hand, it is less than a half of $C(K_s,K_m)$ at the onset. At

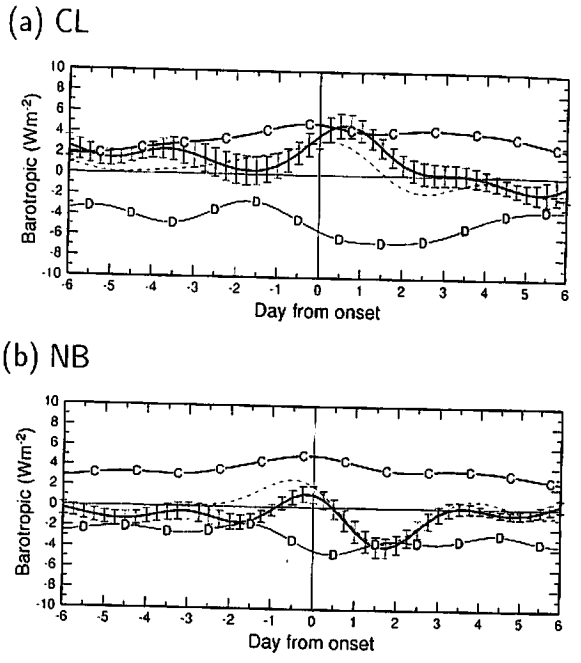

Fig. 7. Time series of the K_m tendency (dashed line), $B(K_m+\phi_m)$ (thick solid line), $C(K_s,K_m)$ (labeled "C") and the residual dissipation term, $D(K_m)$ (labeled "D") for (a) CL and (b) NB composites. All values are averaged in the ridge area ranged from −30° to 45° in longitude, and from 50°N to 80°N in latitude. As for $B(K_m+\phi_m)$, the bars of standard error are also represented.

day +2, it reaches the minimum value (about −4 Wm^{-2}), which is comparable to $C(K_s,K_m)$, but the opposite sign.

6. Discussion and conclusions

In this study, local energetics analysis is conducted for the blocking formation in the North Pacific, in order to investigate the condition of a transient ridge to become a blocking. The total of 452 low-index events are extracted during the 51 winters from 1950 to 2001, using the index of Lejenäs and Økland (1983). Among those, 88 and 253 events are identified as blocking and non-blocking events, respectively. The B-index and C-index are defined to measure the intensity of the low-index events, and the barotropic-baroclinic interactions, respectively.

We first examined the distribution of the low-

index events, plotted as functions of the duration of the low-index events, and the value of the C-index. As a result, we showed the fact that the larger the C-index is, the stronger the blocking ridge grows. A blocking becomes Ω type for large C-index (CL), it becomes dipole type for medium C-index (CM), and the blocking is evanescent for small C-index (CS).

However, there are cases of non-blocking events, in spite of the large values of the C-index. In order to investigate the condition for a transient ridge to become a blocking, we compared the comprehensive kinetic energy budget for the blocking, and non-blocking cases, for the large value of the C-index. The energetics analysis is performed in the framework of the vertical mean and sheared flows, including the barotropic-baroclinic interactions, $C(K_s, K_m)$, and the flux convergence of mechanical energy of the mean flow, $B(K_m + \phi_m)$.

According to the result of the kinetic energy budget, two main differences between CL and NB are found; (1) a positive contribution of $B(K_m + \phi_m)$ around the ridge in CL and a negative in NB, and (2) larger decrease of K_m due to $B(K_m + \phi_m)$ around the upstream jet in CL. In CL, it is thought that K_m generated in the upstream jet is transported eastward and converged around the ridge, and the double-jet structure is formed. Interestingly, K_m around the upstream jet in CL was enhanced prior to the onset time (about day −2), which is consistent with the finding of Tsou and Smith (1990). In NB, on the other hand, it is shown that a poor supply of K_m from the upstream jet, and the negative $B(K_m + \phi_m)$, prevent a transient ridge to develop into a blocking. Therefore, it is concluded that the sign of the flux convergence of mechanical energy around the transient ridge is the condition for the ridge to become a blocking.

Nakamura et al. (1997) examined the roles of high-frequency disturbances, and low-frequency waves, for the formation of blocking. They revealed that the contributions for high-frequency eddies were significant for the Pacific blocking. They also showed that the role of low-frequency waves was not negligible, using the wave activity flux. However, we cannot distinguish the synoptic eddy, and the low-frequency variability in this study. Further studies will be required.

Acknowledgments

The authors thank Dr. T. Yasunari, Dr. F. Kimura, and Dr. H. Ueda for several words of helpful advice and guidance. We are also thankful to the reviewers for their helpful comments. All figures are drawn by the Generic Mapping Tools (GMT) Graphics (Wessel and Smith 1991).

References

Chen, T.-C. and Y.-H. Lee, 1983: A study of the kinetic energy generation with general circulation models. *J. Meteor. Soc. Japan*, **61**, 439–448.

——— and M.-C. Yen, 1985: A note on the kinetic energy budget analysis of the atmospheric baroclinic and barotropic flows. *J. Meteor. Soc. Japan*, **63**, 685–693.

Haines, K. and J. Marshall, 1987: Eddy-forced coherent structures as a prototype of atmospheric blocking. *Quart. J. Roy. Meteor. Soc.*, **113**, 681–704.

Hansen, A.R. and A. Sutera, 1984: A comparison of the spectral energy and enstrophy budgets of blocking versus nonblocking periods. *Tellus*, **36A**, 52–63.

Kalnay, E., M. Kanamitsu, R. Kistler, W. Collins, D. Deaven, L. Gandin, M. Iredell, S. Saha, G. White, J. Woollen, Y. Zhu, M. Chelliah, W. Ebisuzaki, W. Higgins, J. Janowiak, K.C. Mo, C. Ropelewski, J. Wang, A. Leetmaa, R. Reynolds, R. Jenne and D. Joseph, 1996: The NCEP/NCAR 40-year reanalysis project. *Bull. Amer. Meteor. Soc.*, **77**, 437–471.

Kasahara, A. and K. Puri, 1981: Spectral representation of three-dimensional global data by expansion in normal mode functions. *Mon. Wea. Rev.*, **109**, 37–51.

Kimoto, M., H. Mukougawa and S. Yoden, 1992: Medium-range forecast skill variation and blocking transition: A case study. *Mon. Wea. Rev.*, **120**, 1616–1627.

Kung, E.C. and W.E. Baker, 1986: Spectral energetics of the observed and simulated Northern Hemisphere general circulation during blocking episodes. *J. Atmos. Sci.*, **43**, 2792–2812.

Lejenäs, H. and H. Økland, 1983: Characteristics of Northern Hemisphere blocking as determined from a long time series of observational data. *Tellus*, **35A**, 350–362.

Mullen, S.L., 1987: Transient eddy forcing of blocking flows. *J. Atmos. Sci.*, **44**, 3–22.

Nakamura, H. and J.M. Wallace, 1993: Synoptic behavior of baroclinic eddies during the blocking onset. *Mon. Wea. Rev.*, **121**, 1892–1903.

———, M. Nakamura and J.L. Anderson, 1997: The role of high- and low-frequency dynamics in blocking formation. *Mon. Wea. Rev.*, **125**, 2074–2093.

Shutts, G.J., 1983: The propagation of eddies in diffluent jetstreams: Eddy vorticity forcing of 'blocking' flow fields. *Quart. J. Roy. Meteor. Soc.*, **109**, 737–761.

Tanaka, H.L., 1985: Global energetics analysis by expansion into three-dimensional normal mode functions during the FGGE winter. *J. Meteor. Soc. Japan*, **63**, 180–200.

———, 1998: Numerical simulation of a life-cycle of atmospheric blocking and the analysis of potential vorticity using a simple barotropic model. *J. Meteor. Soc. Japan*, **76**, 983–1008.

——— and E.C. Kung, 1988: Normal mode energetics of the general circulation during the FGGE year. *J. Atmos. Sci.*, **45**, 3723–3736.

Tsou, C.-H. and P.J. Smith, 1990: The role of synoptic/planetary-scale interactions during the development of a blocking anticyclone. *Tellus*, **42A**, 174–193.

Watarai, Y. and H.L. Tanaka, 2002: Characteristics of barotropic-baroclinic interactions during the formulation of blocking events in the Pacific region. *J. Meteor. Soc. Japan*, **80**, 387–402.

Wessel, P. and W.H.F. Smith, 1991: Free software helps map and display data. *EOS Trans. Amer. Geophys. U.*, **72**, 445–446.

Wiin-Nielsen, A., 1962: On transformation of kinetic energy between the vertical shear flow and the vertical mean flow in the atmosphere. *Mon. Wea. Rev.*, **90**, 311–323.